Laser ablation for non-destructive sampling of microplastics in single-particle ICP-mass spectrometry

Thibaut Van Acker, Ana Rua-Ibarz[#], Frank Vanhaecke, Eduardo Bolea-Fernandez[#]*

Ghent University, Department of Chemistry, Atomic & Mass Spectrometry – A&MS research group, Campus Sterre, Krijgslaan 281-S12, 9000 Ghent, Belgium

ABSTRACT: In this work, laser ablation (LA) was characterized as a method for sampling and introducing microplastic particles (MPs) into an inductively coupled plasma (ICP) for subsequent $^{13}C^+$ monitoring using an ICP-mass spectrometer operated in single-event mode. MPs of different types (PS, PMMA and PVC) and sizes (2-20 µm) were introduced intactly. The laser energy density did not affect the particle sampling across a wide range (0.25-6.00 J cm^{-2}). Single-shot analysis separated clustered MPs (2-7 MPs per cluster) during the LA and particle transport processes, allowing temporally resolved analysis of the individual constituting MPs. Line scanning showed superior performance when using a small laser beam diameter combined with a high repetition rate. The $^{13}C^+$ signal intensity correlated linearly (R^2 >0.9945) with the absolute C mass in a 2-10 µm size range, while the use of He in the collision-reaction cell (CRC) allowed extension of the linear range to 20 µm. The LA approach generated narrower $^{13}C^+$ signal distributions than the traditional solution-based approach (dry versus wet plasma conditions) and proved successful for the analysis of a mixed suspension (containing 4 sizes of PS MPs in a 2 – 5 µm size range) and for sampling MPs from PVDF and glass microfiber filters, with the latter offering a lower background.

The occurrence of microplastics (MPs, size range 1-5,000 µm) in various environmental compartments and foodstuff is a matter of significant concern.[1] These MPs primarily originate from plastic waste degradation[2] and the smaller of these particles (<10 µm) have often been overlooked in previous assessments due to the lack of adequate analytical methodologies.[3,4]

Various techniques are available for the detection, quantification, and property analysis of MPs within a sample. These encompass microscopic methods, such as transmission electron microscopy (TEM) and scanning electron microscopy (SEM), light scattering techniques like dynamic light scattering (DLS) and multi-angle light scattering (MALS), as well as nanoparticle tracking analysis (NTA), Fourier-transform infrared FT-IR microscopy, Raman microscopy, and pyrolysis-gas chromatography/mass spectrometry (pyr-GC/MS).[5,6] Each subgroup of techniques offers specific insights, while presenting its own set of limitations, highlighting the gap between the requirements and capabilities of current approaches when characterizing MPs at environmentally relevant levels, particularly within the 1 to 10 µm size range.[7–9]

In 2020, single-particle inductively coupled plasma-mass spectrometry (SP-ICP-MS) was demonstrated capable of detecting and quantifying MPs down to 1 µm.[10] This approach provides information on the size distribution (spherical equivalent diameter), mass concentration, and particle number density and is based on monitoring the signal intensity for $^{13}C^+$. Subsequent research confirmed the potential of SP-ICP-MS in this context (monitoring either $^{13}C^+$ or $^{12}C^+$), although also some limitations, including a high carbon background and the need for sample preconcentration due to low MP concentrations in real samples, were realized.[11–14] Although filtration is a common preconcentration method, resuspending the MPs in solution for adequate sample introduction prior to SP-ICP-MS analysis remains challenging.

The combination of laser ablation (LA) for sample introduction and SP-ICP-MS for spatially resolved analysis of metallic nanoparticles in biomaterials was introduced by Metarapi *et al*.[15] and is based on low-energy LA scanning and monitoring the transient signal using a fast-scanning ICP-MS unit.

In this work, a method for sampling individual MPs using LA for their subsequent introduction into the ICP ion source while monitoring the corresponding transient $^{13}C^+$ signal with an ICP-MS instrument operated in single-particle mode has been developed and characterized. Successful release of intact MPs – of different polymer types and within a size range of 2-20 µm diameter – from glass and filter substrates has been achieved using nanosecond laser pulses from a 193 nm excimer-based ArF* laser. This approach was also demonstrated capable of directly sampling MP particles from a filter membrane.

EXPERIMENTAL SECTION

Instrumentation

All measurements were carried out using an Iridia LA-unit (Teledyne Photon Machines, USA) coupled to an Agilent 8900 tandem ICP-MS instrument (ICP-MS/MS, Agilent Technologies, Japan). The LA-unit was equipped with a nanosecond 193 nm ArF* excimer-based laser (MLase, Germany) and a Cobalt ablation chamber with "cup-type" cell.[16] The low-dispersion aerosol transport system ARIS was used to couple the LA-unit to the ICP-MS/MS instrument.[17] The ARIS consists of 0.5 m long and 1 mm inner diameter PEEK tubing and a mixing bulb for the co-axial addition of Ar make-up gas to the He carrier gas flow, transporting the dry aerosol from the ablation site into the ICP. In this work, the ICP-MS/MS instrument was exclusively operated in single quadrupole (SQ) mode, whereby Q1 was used as an ion guide (no mass filtering).[18] For extending the linear dynamic range to larger MPs, the $^{13}C^+$ signal intensity was suppressed by pressurizing the

octupole collision/reaction cell (CRC) with He (1-3 mL min^{-1}). The LA-ICP-MS/MS instrument settings and data acquisition parameters used throughout the work are listed in Tables S1-S9. The instrument settings were fine-tuned daily using NIST SRM 612 glass reference material (National Institute of Standards and Technology, USA) to achieve high signal-to-noise (S/N) ratios across the elemental mass range, low levels of oxide formation ($^{238}U^{16}O+/^{238}U^{+}$ <0.5%) and low elemental fractionation ($^{238}U^{+}/^{232}Th^{+} \approx 1$). Additionally, specific attention was also paid to achieving a high S/N ratio for $^{13}C^{+}$.

Reagents and standards

The CRC was pressurized with pure He (99.9999%, ALPHAGAZ™ 2, Air Liquide, Belgium). A Milli-Q Element water purification system (Millipore, France) was used to produce ultra-pure water (resistivity > 18.2 MΩ cm). Pro analysis purity level 14 M HNO_3 (ChemLab, Belgium) was further purified by sub-boiling distillation. A gelatin droplet standard containing 100 µg g^{-1} Al and Zn was prepared, following the protocol described by Šala *et al.*[19] and used for determining the average peak profiles upon LA of a C-based material (SI).

MP suspensions in deionized water were supplied by Lab261 (USA) and Bangs Laboratories (USA). Different types of polymers, *i.e.* polystyrene (PS, mass density 1.05 g cm^{-3}), polymethylmethacrylate (PMMA, mass density 1.19 g cm^{-3}), and polyvinyl chloride (PVC, mass density 1.38 g cm^{-3}), in a size range from 2 to 20 µm (Table 1), were studied. All MP suspensions were appropriately diluted in Milli-Q water.

Table 1. Standard solutions of PS, PMMA and PVC MPs.

Polymer	Particle diameter (µm)	Particle concentration (particles mL^{-1})
PS	2.07 ± 0.15	2.10 x 10^{10}
	3.10 ± 0.03	6.11 x 10^{8}
	3.97 ± 0.06	2.91 x 10^{8}
	5.19 ± 0.51	1.35 x 10^{9}
	6.05 ± 0.10	8.21 x 10^{7}
	8.12 ± 0.12	3.40 x 10^{7}
	9.87 ± 0.13	1.89 x 10^{7}
	20.15 ± 1.67	2.22 x 10^{6}
PMMA	2.96 ± 0.09	6.19 x 10^{8}
	5.25 ± 0.25	1.11 x 10^{8}
	6.20 ± 0.20	6.73 x 10^{7}
	7.52 ± 0.12	3.77 x 10^{7}
	10.22 ± 0.30	1.50 x 10^{7}
	20.80 ± 1.76	1.78 x 10^{6}
PVC	2.62 ± 0.18	7.70 x 10^{8}
	3.69 ± 0.29	2.75 x 10^{8}
	5.59 ± 0.51	7.92 x 10^{7}

Droplets of 10 µL were spotted on Superfrost™ microscope slides after appropriate dilution to ±10^{6} particles/mL with ultra-pure water. These droplets were dried inside a closed Petri dish in a drying oven at 50 °C. No specific attention was paid to achieving a homogenous distribution of the MPs. Similar droplets were spotted on two different types of filters: polyvinylidene fluoride (PVDF) membrane syringe filters (0.2 µm pore size, Acrodisc, Pall Life Science, Belgium) and high-purity quartz (SiO_2) microfiber filters (0.3 µm pore size, Whatman QM-C pre-fired, UK) without any binder or organic chemicals.

Data processing software and peak detection

HDIP v1.8.4 was used for processing the data exported from the MassHunter software of the Agilent 8900 ICP-MS/MS unit. These data were synchronized with the laser timings listed in the log files generated by the LA operating software (Chromium v3.1). After gas blank subtraction from the transient $^{13}C^{+}$ signal, the build-in peak detection tool[20] was used to distinguish particle events, calculate peak areas and widths for all these events, and construct average peak profiles. Particles were detected with a $n * SD$ detection threshold (with SD the standard deviation of the transient $^{13}C^{+}$ signal and $n = 5 - 12$, depending on the experiment). For further data processing and preparation of figures MATLAB was used.

RESULTS AND DISCUSSION

Comparison of $^{13}C^{+}$ peak profiles obtained upon detection of MPs via LA-SP-ICP-MS and SP-ICP-MS

In order to assess whether MPs can be released from a glass microscope slide as intact entities using LA, experiments were designed to compare single pulse response (SPR) profiles, *i.e.* the transient signal monitored upon an individual laser pulse, directed at different solid sample matrices, e.g., NIST SRM 612 glass, multi-element spiked gelatin droplets and ERM-EC680m PE on the one hand, and individual MPs (3 and 6 µm PS beads) deposited on a microscope slide on the other. **Figure 1A** displays the average SPRs for different matrices with the same LA-ICP-MS setup used throughout this work. All matrices were ablated with a beam of 20 µm diameter, energy density of 3.5 J cm^{-2}, repetition rate of 1 Hz, scan speed of 4 µm s^{-1} and integration time of 3 ms. By normalizing the signal intensities, the shape and duration of the SPRs can be directly compared. The duration of the SPRs observed upon ablation of NIST SRM 612 glass is in the range of 5 ms ($^{27}Al^{+}$, defined as full peak width at 1% of the maximum peak height, FW0.01M) for this setup. For the C-based materials, element-specific peak profiles are generated, as some elements, such as Al, are mainly transported in particulate phase (FW0.01M approx. 20 ms) while others are partially transported in the gaseous phase as well (two-phase sample transport), giving rise to double peaks with a total SPR duration of approximately 100 ms, as illustrated for $^{66}Zn^{+}$ and $^{13}C^{+}$ upon ablation of gelatin and ERM-EC680m PE, respectively.

In SP-ICP-MS, the duration of signal peak profiles obtained upon detection of individual metallic nanoparticles and MPs is around 500 µs.[21] To adequately register such short transient peaks, the integration time was decreased to the instrumental minimum of 100 µs (Table S1). Upon firing laser pulses at individual MPs, originally present in a droplet spotted on a glass microscope slide, it can be observed visually with the LA-unit's microscopic camera that the particles are catapulted from the surface, which is likely the result of the shockwave produced during the LA process. The particles are taken up in and transported away with the He carrier gas via the ablation cell and transport tubing towards the ICP to

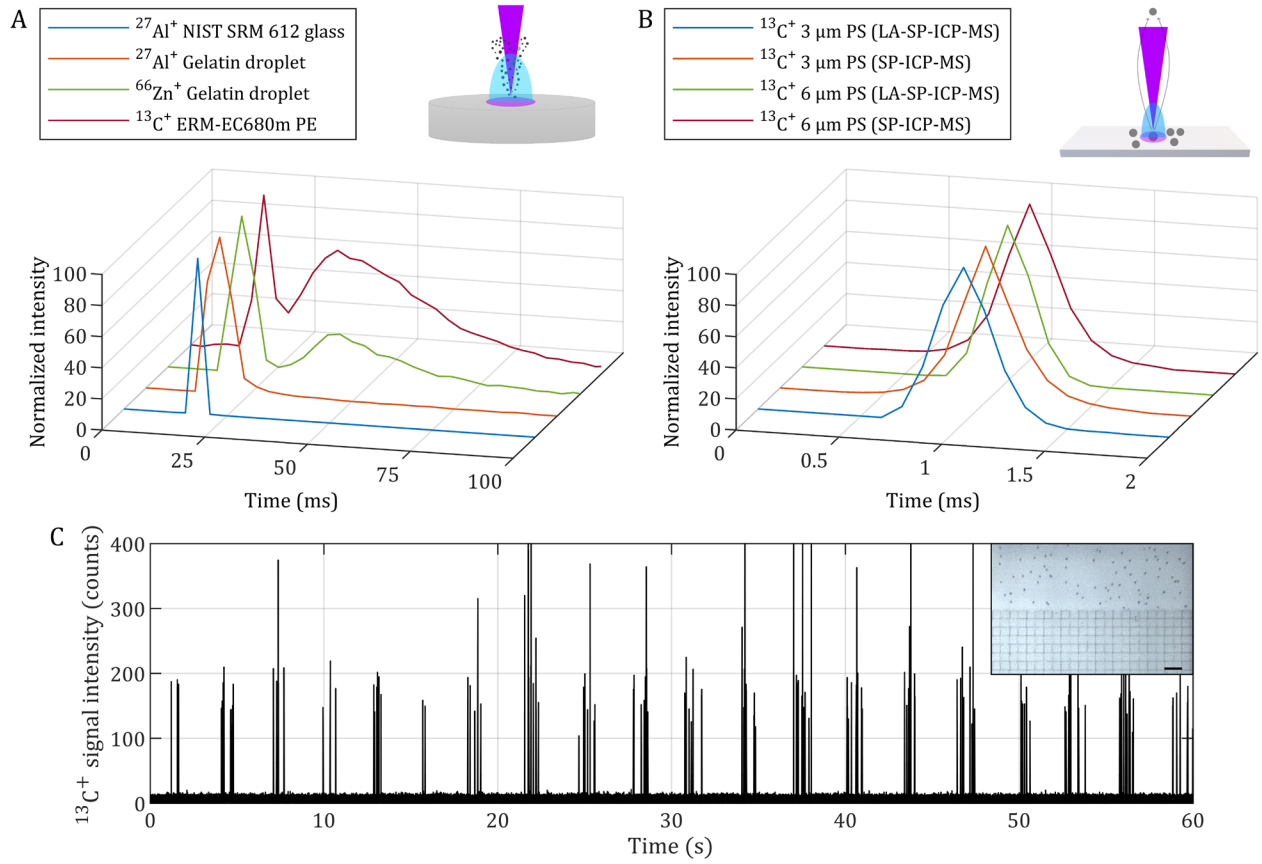

Figure 1. (A) Average SPRs (N = 100) obtained upon ablation of NIST SRM 612 glass ($^{27}Al^+$, blue), a multi-element gelatin droplet ($^{27}Al^+$ and $^{66}Zn^+$, orange and green) and ERM-EC680m PE ($^{13}C^+$, red). (B) Average peak profiles for $^{13}C^+$ obtained upon detection of individual MPs (3 and 6 µm PS) in LA-SP-ICP-MS (blue and green) and SP-ICP-MS (orange and red). (C) Transient $^{13}C^+$ signal upon analysis of 4 µm PS MPs (droplet spotted on a glass microscope slide) via line scanning LA-SP-ICP-MS, with accompanying brightfield LA-unit camera image capturing a portion of the droplet (scale bar = 40 µm).

subsequently undergo vaporization, atomization and ionization, giving rise to much narrower $^{13}C^+$ SPRs than if these particles were vaporized or disintegrated during the LA process. In **Figure 1B**, the average $^{13}C^+$ peak profiles obtained for 3 and 6 µm PS MPs using LA-SP-ICP-MS are compared to those obtained using SP-ICP-MS upon introducing a liquid suspension of MPs. Both approaches reveal identical peak profiles in terms of shape and duration, strongly suggesting that these particles enter the ICP as intact MPs using LA for sampling. Additionally in **Figure 1C**, an exemplary $^{13}C^+$ transient signal monitored upon ablating multiple line scans on a dried droplet containing 4 µm PS MPs is displayed.

Effect of laser energy density on particle integrity

To evaluate the effect of the laser energy density on potential particle disintegration, seven laser energy densities were selected (0.10, 0.25, 0.50, 1.00, 2.00, 4.00 and 6.00 J cm^{-2}), and for each, three line scans were ablated on a dried droplet containing 5 µm PS MPs using a 10 µm diameter fired at a repetition rate of 125 Hz. The number of particles detected in case of the lowest laser energy density applied (0.10 J cm^{-2}) was only 13, but upon increasing the laser energy density, the number of particles detected increased and further remained relatively constant across a wide range, with 109, 113, 102, 106, 97 and 117 (107±8 particles detected), respectively. In **Figure 2**, the average $^{13}C^+$ integrated signal intensities and peak widths have been plotted as a function of the laser energy density along with overall population averages and standard deviations (4,850±913 counts and 0.47±0.04 ms). Both $^{13}C^+$ integrated signal intensities and peak widths remain constant with increasing laser energy density, indicating that the MPs remain intact after LA sampling and are introduced into the ICP as discrete entities.

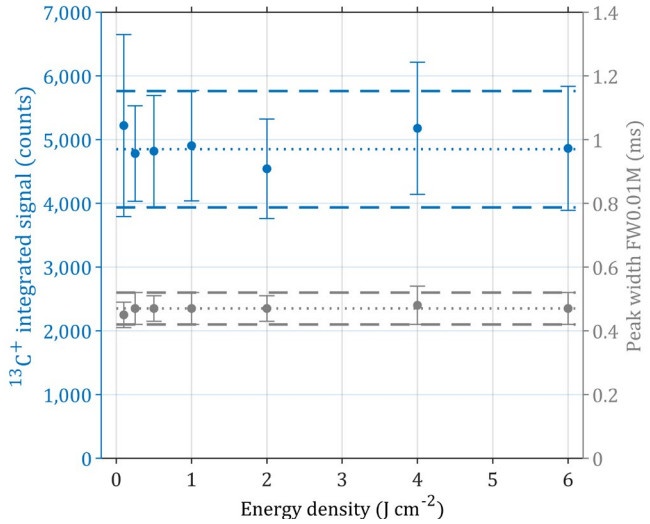

Figure 2. Average integrated $^{13}C^+$ signal intensities (±SD, left y-axis, blue) and peak widths defined as FW0.01M (±SD, right y-axis, grey) as a function of the laser energy density for 5 µm di-

ameter PS MPs. In both cases, also population averages (dotted lines) and corresponding uncertainties (±SD, dashed lines) are displayed.

Single shot analysis of clustered MPs and line scanning approach

An important aspect of SP-ICP-MS is to limit the number of double events affecting measurement accuracy; ideally all particles are detected individually and if the percentage of double events is too high, the suspension can be diluted to limit the number of particles introduced per unit of time.[22] For LA-SP-ICP-MS analysis, in addition to diluting the initial suspension, there is the possibility to balance the laser beam size, as well as the repetition rate, rendering it a flexible sample introduction system for discrete entities. In SP-ICP-MS, it is also important to vortex and sonicate the suspension to avoid particle agglomeration which would lead to a high degree of double events. In LA-SP-ICP-MS, agglomerated or clustered particles can also occur, and single shot analyses were performed on clustered MPs to evaluate whether the technique would be capable of separating these MPs in time and space during ablation and transport towards the ICP. **Figure 3** displays the results of single shot analyses performed on clustered MPs (6 µm PS) deposited on a microscope slide. Brightfield camera images show 2 to 7 clustered MPs before analysis and what is left afterwards. It can be seen that MPs located inside the target regions (blue circles) are set free from the microscope slide, while other MPs remain on the slide. The number of $^{13}C^+$ peaks in the transient signal corresponds to the original number of MPs in the clusters. This means that even MPs that were initially agglomerated can be released from the slide and end up in the central channel of the ICP at different times, sometimes even with tens of ms difference in arrival time. It is highly likely that upon laser pulse impact, the particles are separated from one another due to the shockwave and further separation occurs in the transport tubing between the ablation cell and ICP.

To sample a higher number of MPs per unit of time and scan larger areas, a line-by-line scanning approach is preferred over spot (point-by-point) analysis. High lateral scan speeds up to 5 mm s^{-1} can be achieved with state-of-art LA units. For line scanning, it was observed that firing at higher repetition rate combined with a smaller laser beam diameter is preferred over a lower repetition rate combined with a larger beam diameter. Highly agglomerated clusters of MPs can be released at once using large laser beam diameters, leading to more double events, while with a small laser beam diameter only a few MPs of these highly agglomerated clusters are released per shot. As an example, two identical areas (1,750x50 µm²) on a microscope slide containing 4 µm PS MPs were analyzed with two different combinations of LA settings (SI video 1). One area was analyzed using 5 line scans with a 10 µm diameter laser beam at 125 Hz repetition rate (1 shot per position and lateral scan speed of 1.25 mm s^{-1}), the other using 1 line scan with a 50 µm diameter laser beam at 5 Hz (1 shot per position and lateral scan speed of 0.25 mm s^{-1}). The rate of double events detected increased from 15% to 40% for the large beam diameter and low repetition rate combination. The total number of particles detected, taking into account the double events, was highly comparable between both areas (139 and 131).

Linearity between the $^{13}C^+$ signal and particle volume for PS, PMMA and PVC MPs

One of the *a priori* concerns of MP analysis using (LA-)SP-ICP-MS, is the potential lack of linearity between the integrated $^{13}C^+$ signal and the particle volume, which could occur as a result of incomplete vaporization, atomization and ionization of larger sized MPs in the ICP ion source, as has already been observed in the context of SP-ICP-MS analysis of AuNPs.[23] Therefore, a wide range of MP sizes was considered.

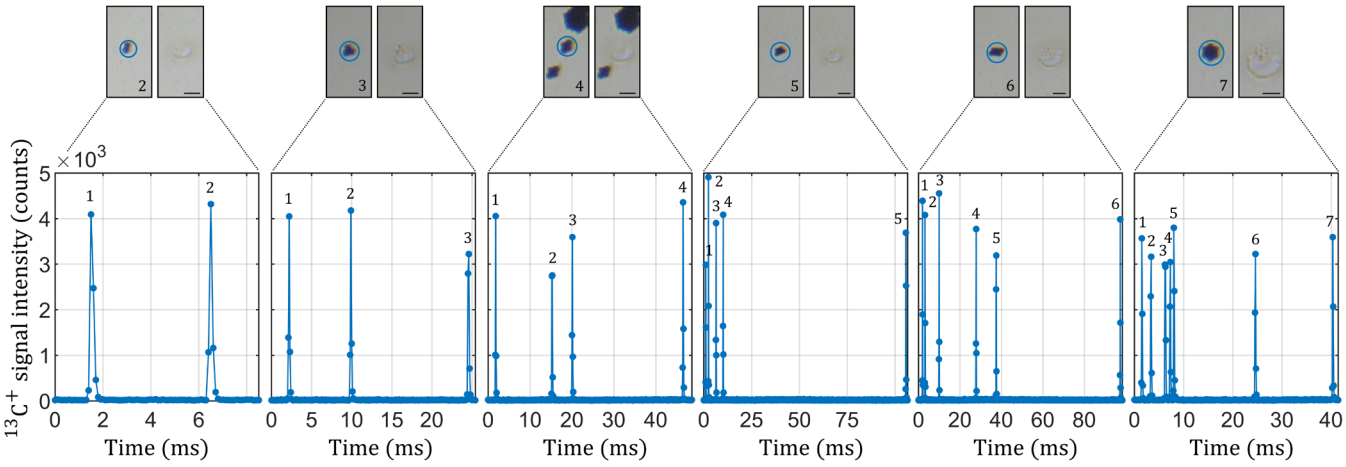

Figure 3. Brightfield camera images of 2 to 7 clustered MPs (6 µm PS) before single shot analysis and of what is left after analysis with resulting $^{13}C^+$ transient signal peaks monitored using an integration time of 100 µs.

With the CRC operated in vented mode (no gas), small areas of dried droplets, containing 2-10 µm PS MPs and deposited on a microscope slide, were ablated line-by-line and the average $^{13}C^+$ signal intensity was plotted as a function of the particle volume, which yielded a highly linear correlation (R^2 = 0.9990) – see **Figure 4**. Under the same experimental conditions, also for 3-10 µm PMMA MPs and 3-6 µm PVC MPs, a highly linear response was obtained (R^2 = 0.9945 and 1.0000 for PMMA and PVC, respectively). The slopes of all 3 linear regression lines were derived (27.40, 19.46 and 13.68 counts $µm^{-3}$ for PS, PMMA and PVC, respectively) and used to verify whether the $^{13}C^+$ signal intensities monitored were affected by

polymer type. Ideally, the $^{13}C^+$ signal is proportional to the absolute mass of C in the MPs and is independent of the polymer type. The C content in PS, PMMA and PVC is 92.3, 60.0 and 38.7%, respectively, and thus theoretically, taking into account the mass densities, a PS MP of a specific size should yield a 1.4-fold higher $^{13}C^+$ signal than a PMMA MP of the same size and a 1.8-fold higher $^{13}C^+$ signal than a PVC MP of the same size. The values derived by dividing the slope of the PS linear regression line by that of PMMA and PVC, yield ratios of 1.4 and 2.0, in good agreement with the theoretical values (1.4 and 1.8). Size detection limits of 0.9, 1.0 and 1.2 µm were achieved for PS, PMMA and PVC, respectively, and were in good agreement with previous studies (SI).[10–12]

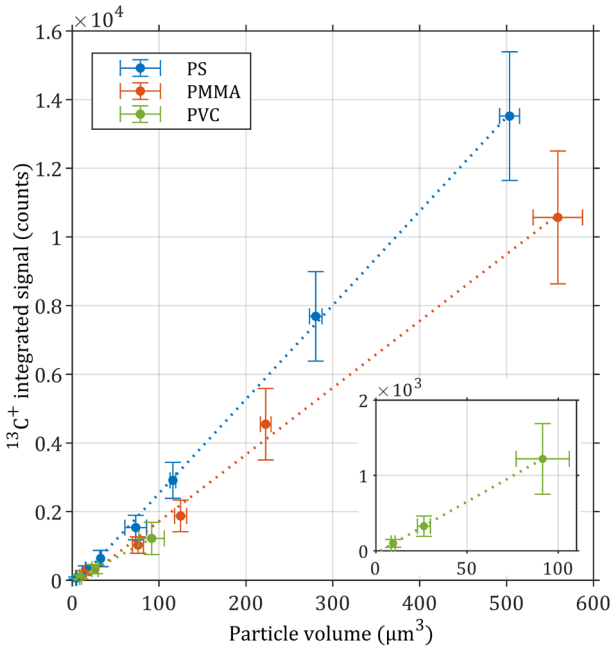

Figure 4. Average $^{13}C^+$ signal intensity as a function of particle volume for PS, PMMA and PVC) MPs originally present in a droplet spotted on a microscope slide and analyzed via LA-SP-ICP-MS (N = 400-500 particles).

These results demonstrate that even MPs of 10 µm diameter are handled adequately by the ICP under these conditions. However, as can be seen in **Figure 5A**, analysis of even larger particles, 20 µm diameter PS and PMMA MPs, did not yield a linear response anymore in pulse-counting mode, most likely due to overlapping ions arriving at the detector within the dead time of the electron multiplier. Therefore, the sensitivity was decreased by pressurizing the CRC with 3.0 mL min^{-1} He as collision gas, while also the effect of the Ar make-up gas flow rate on the $^{13}C^+$ signal intensities was evaluated for 10 and 20 µm MPs, as it has a significant influence on the residence time of the MPs in the ICP. On the left y-axis of **Figure 5B**, the average integrated $^{13}C^+$ signals for 10 and 20 µm PS MPs are displayed versus the Ar make-up gas flow rate and on the right y-axis, the ratios of the $^{13}C^+$ integrated signals for 20 µm and 10 µm MPs are plotted. Also, the theoretical ratio of 8.51±0.71, calculated based on the corresponding particle volumes, is indicated. One can observe that the experimental ratio varies largely (1.5-19) and that at 0.90 L min^{-1}, the $^{13}C^+$ signal reaches its maximum for 20 µm MPs and the experimental and theoretical ratios are in good agreement. At higher gas flow rates, the experimental ratio is lower than the theoretical one as a result of insufficient residence time in the ICP for complete particle vaporization, atomization and ionization for 20 µm MPs, as signaled by the significant drop in $^{13}C^+$ signal. At lower gas flow rates, the experimental ratio exceeds the theoretical ratio which could be explained by 20 µm MPs having sufficient residence time in the ICP for complete particle vaporization but with the zone of maximum $^{13}C^+$ ion density for the 10 µm MPs located too much upstream in the ICP (too close to the rf coil), such that it is not efficiently sampled by the sampling cone.[24]

Comparison of the $^{13}C^+$ signal distributions for wet versus dry plasma conditions (SP-ICP-MS versus LA-SP-ICP-MS) and analysis of mixed MPs

Earlier, it was demonstrated that the average SPRs for PS MPs analyzed via SP-ICP-MS and LA-SP-ICP-MS were identical, while the plasma conditions are very different (wet versus dry plasma conditions). When comparing the $^{13}C^+$ signal distributions for MPs (3, 4 and 6 µm PS) in wet (**Figures 6A-C**) and dry plasma conditions (**Figures 6D-F**) for the same number of detected events, the signal distributions for SP-ICP-MS appear broader compared to LA-SP-ICP-MS and this could be attributed to the hypothesis that under dry plasma conditions, the ICP is more powerful and can vaporize, atomize and ionize large particles more easily, which translates into narrower signal distributions. This results in varying sizes being more easily distinguishable. Therefore, the methodology was evaluated in a more complex situation, *i.e.,* the analysis of a mixed suspension containing 2, 3, 4 and 5 µm diameter PS MPs (lower size range) spotted onto a microscope slide. A total of 12 lines were ablated over a time span of 4 min and the transient $^{13}C^+$ signal monitored during 40 s was plotted in **Figure 6G**. A logarithmic scale was selected for the y-axis for better visualization of the peak maxima. After background subtraction and peak detection (N = 2,032 peaks), integrated $^{13}C^+$ signal intensities were obtained, histograms constructed, and normal distributions fitted to the data (**Figure 6H**). Four distinct normal distributions (µ = 72, 306, 673 and 1,551 counts, and SD = 38, 60, 118 and 283 counts, respectively) are observed with some overlap between them. In the figure inset, the means of the distributions with corresponding SDs were plotted as a function of the particle volume and a very good linear correlation was achieved (R^2 = 1.0000). It should be noted that the width of the distribution of the 5 µm PS MPs is slightly broader because of the larger spread in size, e.g., 5.19±0.51 µm (5 µm PS, RSD = 17%) versus 3.97±0.06 µm (4 µm, RSD = 3%).

Sampling MPs on carbon-based and carbon-free filter substrates

All previous experiments were performed on dried suspensions of MPs droplet-spotted onto soda-lime-silica glass microscope slides. To verify whether the MPs could also be released from filter materials, which are regularly used to extract MPs from environmental matrices, e.g., surface water, two different filter types, a C-based PVDF filter and a C-free GMF filter, were used as substrates for deposition of a suspension containing 6 µm PS MPs. Multiple line scans were ablated on both substrates using a 10 µm laser beam diameter, repetition rate of 25 Hz and laser energy density of 2 J cm^{-2}. In **Figure 7A**, the transient $^{13}C^+$ signal monitored is displayed, demonstrating a consistent release and detection of MPs from the GMF filter without elevated $^{13}C^+$ background.

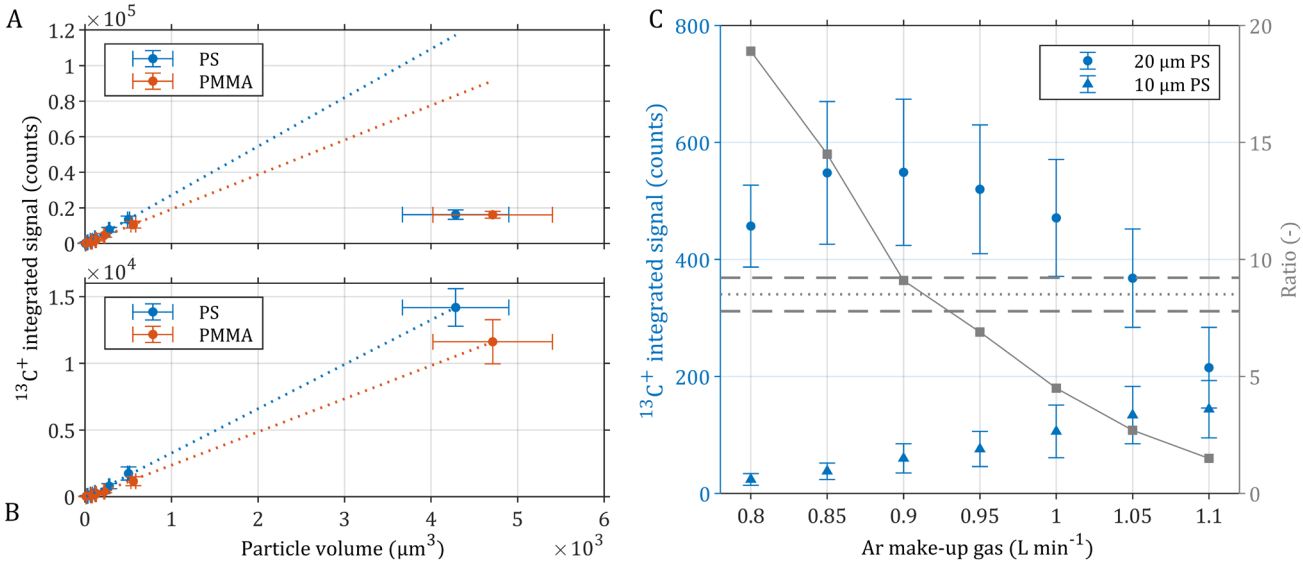

Figure 5. (A) Extrapolation of linear signal intensity vs. particle volume for 20 µm PS and PMMA MPs in vented CRC mode. (B) Linear correlation between $^{13}C^+$ signal intensity and particle volume for PS and PMMA MPs up to 20 µm diameter in He CRC mode (1.2 mL min^{-1}). (C) Effect of Ar make-up gas flow rate on $^{13}C^+$ signal intensities for 10 and 20 µm PS MPs with corresponding experimental ratios of $^{13}C^+$ signal intensities for 20 over those for 10 µm PS MPs and the theoretical ratio (grey dotted line) ± SD (grey dashed lines) in He CRC mode (3 mL min^{-1}).

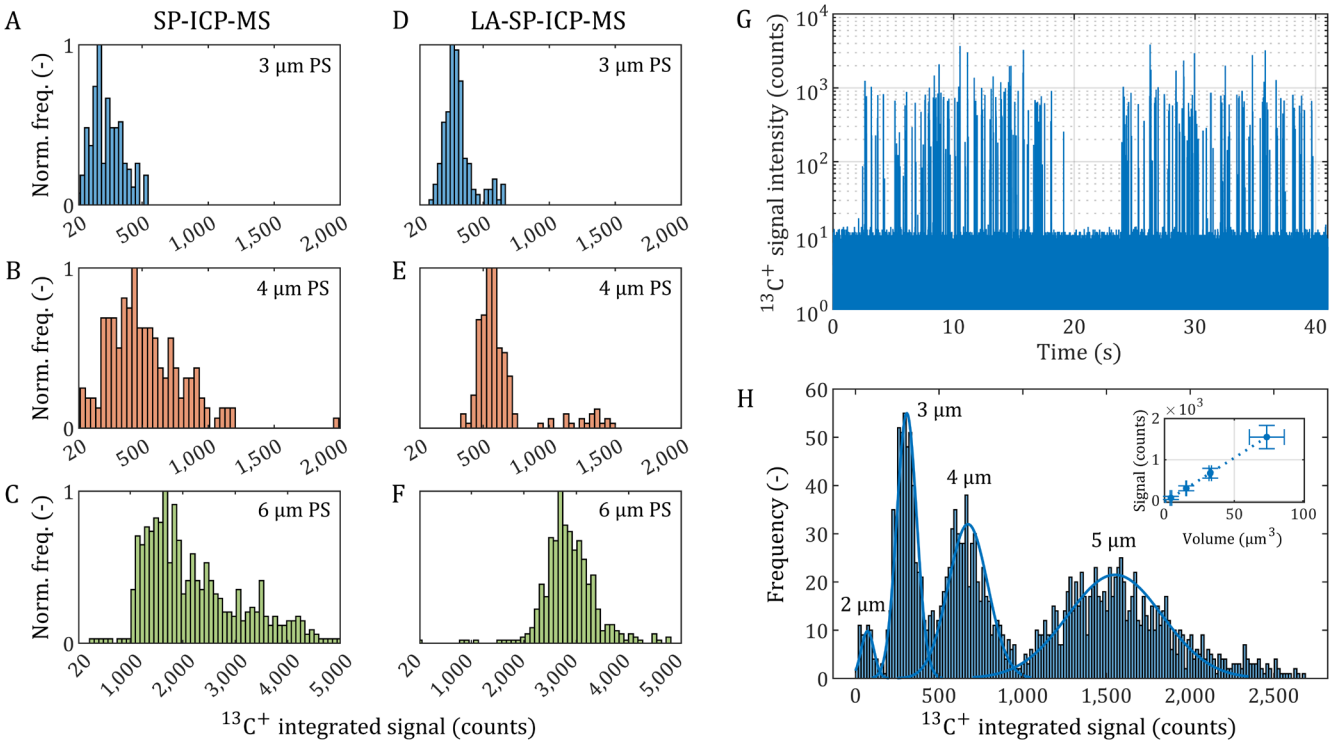

Figure 6. (A-C) $^{13}C^+$ integrated signal distributions as frequency normalized binned histograms for 3, 4 and 6 µm PS MPs analyzed via SP-ICP-MS (wet plasma) and via (D-F) LA-SP-ICP-MS (dry plasma). (G) Transient $^{13}C^+$ signal monitored upon ablation of a mixture of 2, 3, 4 and 5 µm PS MPs and corresponding $^{13}C^+$ integrated distributions with fitted normal distributions for each particle size. Linear correlation between integrated $^{13}C^+$ signal intensity and MP particle volume.

From **Figure 7B**, it is clear that the PVDF filter substrate is partially co-ablated, resulting in transient $^{13}C^+$ peaks. Although the $^{13}C^+$ peaks resulting from the PVDF are of a longer duration than the $^{13}C^+$ peaks arising from individual MPs, particle detection and detection power are compromised due to the elevated background signal. **Figure 7B** shows the superposition of narrow $^{13}C^+$ signal spikes on top of a wider $^{13}C^+$ peak. Even at lower laser energy densities, down to 0.50 J cm^{-2}, significant substrate co-ablation was observed. The transient nature of the $^{13}C^+$ signal originating from co-ablation of the substrate could be minimized by using an LA-setup characterized by a higher dispersion, for example by incorporating mixing bulbs and/or using aerosol transport tubing with wider inner diameter, to mix the aerosol and smooth the signal, but

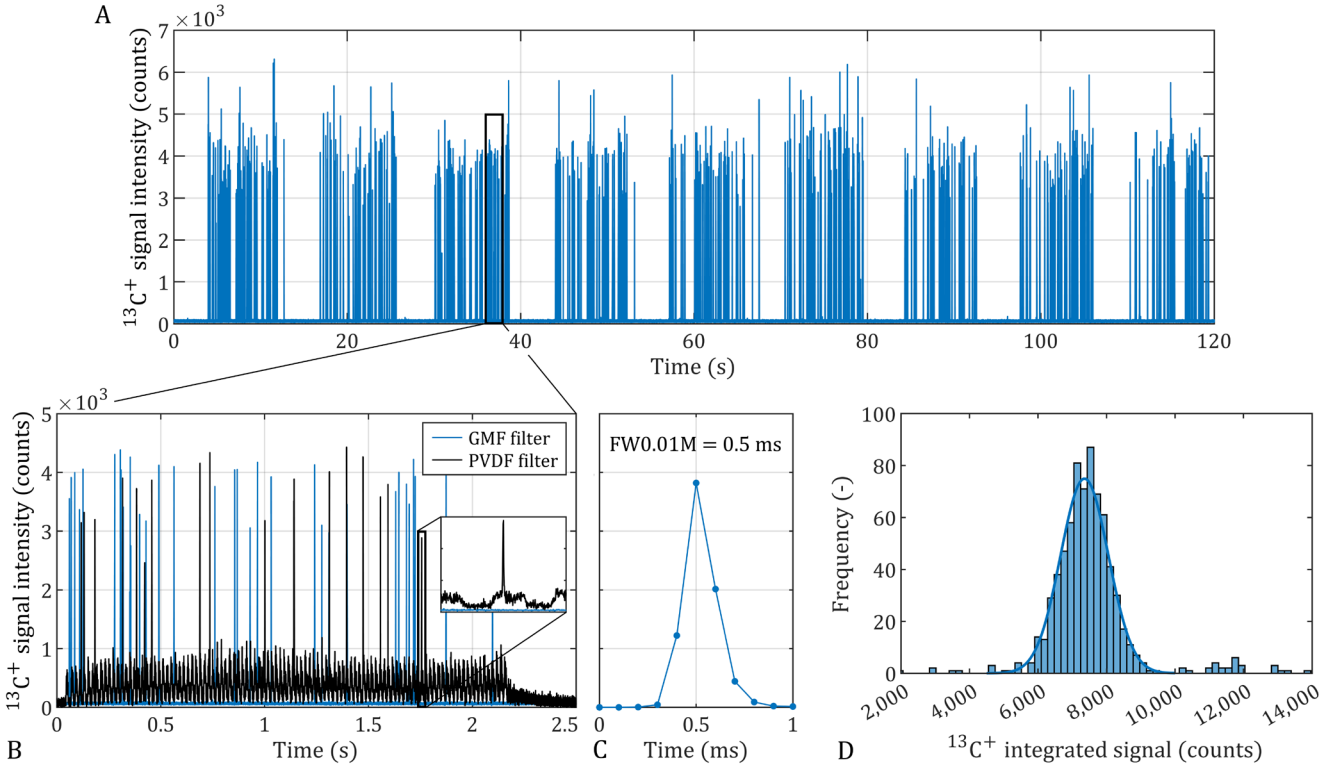

Figure 7. (A) Transient $^{13}C^+$ signal upon ablation of 9 line scans on a dried droplet deposited on a GMF filter containing 6 µm PS MPs. (B) Comparison of transient $^{13}C^+$ signals for analysis of 6 µm PS MPs deposited on a GMF (blue) and PVDF (black) filter with figure inset displaying the $^{13}C^+$ signal contribution originating from co-ablation of the C-based PVDF filter. (C) Resulting average peak profile and (D) binned histogram representing the $^{13}C^+$ signal distribution of 6 µm PS MPs (N = 734).

this in turn can lead to particle losses and thus, decreased particle transport efficiency. **Figures 7C and 7D** display the average peak profiles for 6 µm PS MPs and the frequency distribution as binned histogram and fitted normal distribution. The average peak width (FW0.01M) is 0.5 ms, and this demonstrates that the MPs are also released as intact entities from the GMF filter substrate.

CONCLUSIONS

The potential of LA as a non-destructive sampling method allowing for the introduction of individual intact MPs into the ICP ion source for SP- ICP-MS analysis has been demonstrated. This allowed their detection and quantification in a wide size range (2-20 µm) with a highly linear correlation between the integrated $^{13}C^+$ signal intensity and the absolute mass of C, independently of the MP type (PS, PMMA and PVC). The $^{13}C^+$ signal distributions were narrower for LA-SP-ICP-MS compared to solution-based SP-ICP-MS (dry versus wet plasma conditions), allowing MPs of different sizes to be more easily distinguishable. The approach proved effective in analyzing suspensions containing MPs of various sizes (2-5 µm) and MP suspensions deposited onto different substrates. C-free filter material was proven superior as a result of co-ablation of C-containing filter material. Overall, the LA approach developed is promising as it can offer a solution for characterizing MPs in real samples, even at low concentrations.

ASSOCIATED CONTENT

Supporting Information

Supporting information document available with all instrument settings and data acquisition conditions (.PDF)

Video with screen captures of line scanning approach (.MOV)

AUTHOR INFORMATION

Corresponding Author

*Corresponding author: Eduardo.BoleaFernandez@UGent.be – Tel: +3292644807

Present Addresses

[#]Current affiliation: University of Zaragoza, Aragón Institute of Engineering Research (I3A), Department of Analytical Chemistry, Zaragoza, Spain

Author Contributions

The manuscript was written through contributions of all authors. All authors have given approval to the final version of the manuscript.

ACKNOWLEDGMENT

T.V.A. thanks the Research Foundation Flanders for support from a postdoctoral research fellowship (FWO.3E0.2022.0048.01). A.R.-I. thanks European Union´s Horizon 2020 research and innovation program under the Marie-Sklodowska-Curie grant agreement Nº 101034288. E.B.-F. acknowledges financial support from FWO-Vlaanderen (grants 12ZA320N and 12ZA323N) and from the Ramón y Cajal programme (RYC2021-031093-I) funded by MCIN/AEI/10.13039/501100011033 and the European Union (NextGenerationEU/PRTR), the grant PID2021-122455NB-I00, funded by MCIN/AEI/ 10.13039/501100011033 and by "ERDF A way of making Europe", and also the Aragon Government (DGA, Construyendo Europa desde Aragón, Grupo E43_20R).

REFERENCES

(1) Hale, R. C.; Seeley, M. E.; La Guardia, M. J.; Mai, L.; Zeng, E. Y. A Global Perspective on Microplastics. J. Geophys. Res. Ocean. 2020, 125 (1), 1–40. https://doi.org/10.1029/2018JC014719.

(2) Vethaak, A. D.; Legler, J. Microplastics and Human Health. Science (80-.). 2021, 371 (6530), 672–674. https://doi.org/10.1126/science.abe5041.

(3) Nguyen, B.; Claveau-Mallet, D.; Hernandez, L. M.; Xu, E. G.; Farner, J. M.; Tufenkji, N. Separation and Analysis of Microplastics and Nanoplastics in Complex Environmental Samples. Acc. Chem. Res. 2019, 52 (4), 858–866. https://doi.org/10.1021/acs.accounts.8b00602.

(4) Velimirovic, M.; Tirez, K.; Voorspoels, S.; Vanhaecke, F. Recent Developments in Mass Spectrometry for the Characterization of Micro- and Nanoscale Plastic Debris in the Environment. Anal. Bioanal. Chem. 2021, 413 (1), 7–15. https://doi.org/10.1007/s00216-020-02898-w.

(5) Schwaferts, C.; Niessner, R.; Elsner, M.; Ivleva, N. P. Methods for the Analysis of Submicrometer- and Nanoplastic Particles in the Environment. TrAC Trends Anal. Chem. 2019, 112, 52–65. https://doi.org/10.1016/j.trac.2018.12.014.

(6) Oliveira, M.; Almeida, M. The Why and How of Micro(Nano)Plastic Research. TrAC Trends Anal. Chem. 2019, 114, 196–201. https://doi.org/10.1016/j.trac.2019.02.023.

(7) Caputo, F.; Vogel, R.; Savage, J.; Vella, G.; Law, A.; Della Camera, G.; Hannon, G.; Peacock, B.; Mehn, D.; Ponti, J.; Geiss, O.; Aubert, D.; Prina-Mello, A.; Calzolai, L. Measuring Particle Size Distribution and Mass Concentration of Nanoplastics and Microplastics: Addressing Some Analytical Challenges in the Sub-Micron Size Range. J. Colloid Interface Sci. 2021, 588, 401–417. https://doi.org/10.1016/j.jcis.2020.12.039.

(8) Xu, J.-L.; Thomas, K. V.; Luo, Z.; Gowen, A. A. FTIR and Raman Imaging for Microplastics Analysis: State of the Art, Challenges and Prospects. TrAC Trends Anal. Chem. 2019, 119, 115629. https://doi.org/10.1016/j.trac.2019.115629.

(9) Barbosa, F.; Adeyemi, J. A.; Bocato, M. Z.; Comas, A.; Campiglia, A. A Critical Viewpoint on Current Issues, Limitations, and Future Research Needs on Micro- and Nanoplastic Studies: From the Detection to the Toxicological Assessment. Environ. Res. 2020, 182 (October 2019), 109089. https://doi.org/10.1016/j.envres.2019.109089.

(10) Bolea-Fernandez, E.; Rua-Ibarz, A.; Velimirovic, M.; Tirez, K.; Vanhaecke, F. Detection of Microplastics Using Inductively Coupled Plasma-Mass Spectrometry (ICP-MS) Operated in Single-Event Mode. J. Anal. At. Spectrom. 2020, 35 (3), 455–460. https://doi.org/10.1039/c9ja00379g.

(11) Laborda, F.; Trujillo, C.; Lobinski, R. Analysis of Microplastics in Consumer Products by Single Particle-Inductively Coupled Plasma Mass Spectrometry Using the Carbon-13 Isotope. Talanta 2021, 221 (April 2020), 121486. https://doi.org/10.1016/j.talanta.2020.121486.

(12) Gonzalez de Vega, R.; Goyen, S.; Lockwood, T. E.; Doble, P. A.; Camp, E. F.; Clases, D. Characterisation of Microplastics and Unicellular Algae in Seawater by Targeting Carbon via Single Particle and Single Cell ICP-MS. Anal. Chim. Acta 2021, 1174, 338737. https://doi.org/10.1016/j.aca.2021.338737.

(13) Liu, Z.; Zhu, Y.; Lv, S.; Shi, Y.; Dong, S.; Yan, D.; Zhu, X.; Peng, R.; Keller, A. A.; Huang, Y. Quantifying the Dynamics of Polystyrene Microplastics UV-Aging Process. Environ. Sci. Technol. Lett. 2022, 9 (1), 50–56. https://doi.org/10.1021/acs.estlett.1c00888.

(14) Gao, W.; Zhang, Y.; Mo, A.; Jiang, J.; Liang, Y.; Cao, X.; He, D. Removal of Microplastics in Water: Technology Progress and Green Strategies. Green Anal. Chem. 2022, 3 (September), 100042. https://doi.org/10.1016/j.greeac.2022.100042.

(15) Metarapi, D.; Šala, M.; Vogel-Mikuš, K.; Šelih, V. S.; Van Elteren, J. T. Nanoparticle Analysis in Biomaterials Using Laser Ablation-Single Particle-Inductively Coupled Plasma Mass Spectrometry. Anal. Chem. 2019, 91 (9), 6200–6205. https://doi.org/10.1021/acs.analchem.9b00853.

(16) Van Malderen, S. J. M.; Van Acker, T.; Vanhaecke, F. Sub-Micrometer Nanosecond LA-ICP-MS Imaging at Pixel Acquisition Rates above 250 Hz via a Low-Dispersion Setup. Anal. Chem. 2020, 92 (8), 5756–5764. https://doi.org/10.1021/acs.analchem.9b05056.

(17) Van Acker, T.; Van Malderen, S. J. M.; Van Helden, T.; Stremtan, C.; Šala, M.; van Elteren, J. T.; Vanhaecke, F. Analytical Figures of Merit of a Low-Dispersion Aerosol Transport System for High-Throughput LA-ICP-MS Analysis. J. Anal. At. Spectrom. 2021, 36 (6), 1201–1209. https://doi.org/10.1039/D1JA00110H.

(18) Bolea-Fernandez, E.; Balcaen, L.; Resano, M.; Vanhaecke, F. Overcoming Spectral Overlap via Inductively Coupled Plasma – Tandem Mass Spectrometry (ICP-MS/MS). A Tutorial Review. J. Anal. At. Spectrom. 2017, 32 (9), 1660–1679.

(19) Šala, M.; Šelih, V. S.; van Elteren, J. T. Gelatin Gels as Multi-Element Calibration Standards in LA-ICP-MS Bioimaging: Fabrication of Homogeneous Standards and Microhomogeneity Testing. Analyst 2017, 142 (18), 3356–3359.

(20) Tuoriniemi, J.; Cornelis, G.; Hassellöv, M. Size Discrimination and Detection Capabilities of Single-Particle ICPMS for Environmental Analysis of Silver Nanoparticles. Anal. Chem. 2012, 84 (9), 3965–3972. https://doi.org/10.1021/ac203005r.

(21) Bolea-Fernandez, E.; Leite, D.; Rua-Ibarz, A.; Liu, T.; Woods, G.; Aramendia, M.; Resano, M.; Vanhaecke, F. On the Effect of Using Collision/Reaction Cell (CRC) Technology in Single-Particle ICP-Mass Spectrometry (SP-ICP-MS). Anal. Chim. Acta 2019, 1077, 95–106. https://doi.org/10.1016/j.aca.2019.05.077.

(22) Olesik, J. W.; Gray, P. J. Considerations for Measurement of Individual Nanoparticles or Microparticles by ICP-MS: Determination of the Number of Particles and the Analyte Mass in Each Particle. J. Anal. At. Spectrom. 2012, 27 (7), 1143. https://doi.org/10.1039/c2ja30073g.

(23) Lee, W.; Chan, W. Calibration of Single-Particle Inductively Coupled Plasma-Mass Spectrometry (SP-ICP-MS). 2015, 1245–1254. https://doi.org/10.1039/c4ja00408f.

(24) Vanhaecke, F.; Dams, R.; Vandecasteele, C. 'Zone Model' as an Explanation for Signal Behaviour and Non-Spectral Interferences in Inductively Coupled Plasma Mass Spectrometry. J. Anal. At. Spectrom. 1993, 8 (3), 433–438. https://doi.org/10.1039/JA9930800433.